

## MgSn<sub>0.05</sub>Ti<sub>0.95</sub>O<sub>3</sub>–SrTiO<sub>3</sub>复相陶瓷的显微结构与微波介电性能

龚志杰<sup>1</sup>, 王哲飞<sup>1</sup>, 王丽熙<sup>1</sup>, 韩巍<sup>2</sup>, 付振晓<sup>2</sup>, 张其土<sup>1</sup>

(1. 南京工业大学材料科学与工程学院, 南京 210009; 2. 广东风华高新科技股份有限公司, 广东 肇庆 526000)

**摘要:**采用传统固相法制备了不同摩尔配比的(1-x)MgSn<sub>0.05</sub>Ti<sub>0.95</sub>O<sub>3</sub>-xSrTiO<sub>3</sub>微波介质复相陶瓷材料, 研究了复相陶瓷的烧结特性、显微结构和微波介电性能。结果表明:MgSn<sub>0.05</sub>Ti<sub>0.95</sub>O<sub>3</sub>和SrTiO<sub>3</sub>两相共存, 无固溶现象。随着SrTiO<sub>3</sub>含量的增多,(1-x)MgSn<sub>0.05</sub>Ti<sub>0.95</sub>O<sub>3</sub>-xSrTiO<sub>3</sub>的相对介电常数( $\epsilon_r$ )线性增大, 品质因数( $Q \times f$ )下降, 谐振频率温度系数( $\tau_f$ )从负值变为正值。通过调节x值, 可以获得近零的 $\tau_f$ 值。陶瓷的 $\tau_f$ 变化符合Lichtenegger混合法则。0.98MgSn<sub>0.05</sub>Ti<sub>0.95</sub>O<sub>3</sub>-0.02SrTiO<sub>3</sub>复相陶瓷在1330℃烧结4 h, 获得最佳的微波介电性能: $\epsilon_r=19.32$ ,  $Q \times f=193.527$  THz,  $\tau_f=-2 \times 10^{-6}$ /℃。

**关键词:**微波介质陶瓷; 复相陶瓷; 介电性能; 品质因数

中图分类号:TQ174.75 文献标志码:A 文章编号:0454-5648(2013)01-

网络出版时间: 网络出版地址:

## Microwave Dielectric Properties of MgSn<sub>0.05</sub>Ti<sub>0.95</sub>O<sub>3</sub>–SrTiO<sub>3</sub> Multiphase Ceramics

GONG Zhijie, WANG Zhefei, WANG Lixi, HAN Wei, FU Zhenxiao, ZHANG Qitu

(1. College of Materials Science and Engineering, Nanjing University of Technology, Nanjing 210009, China; 2. Guangdong Fenghua Advanced Technology Company Limited, Guangdong 526020, China)

**Abstract:** The microwave dielectric multiphase ceramics of (1-x)MgSn<sub>0.05</sub>Ti<sub>0.95</sub>O<sub>3</sub>-xSrTiO<sub>3</sub> were prepared by a conventional solid-state route. The sinterability, microstructures and microwave dielectric properties of the multiphase ceramics were investigated. The results show that MgSn<sub>0.05</sub>Ti<sub>0.95</sub>O<sub>3</sub> and SrTiO<sub>3</sub> can co-exist as two phases without any solid solution. The relative dielectric constant ( $\epsilon_r$ ) linearly increased, the quality factor ( $Q \times f$ ) decreased and the value of the temperature coefficient of resonance frequency ( $\tau_f$ ) varied from negative to positive with the increase of SrTiO<sub>3</sub> content. In addition, a near-zero  $\tau_f$  value was obtained by the adjustment of the value of x. The variation in the the value of  $\tau_f$  of (1-x)MgSn<sub>0.05</sub>Ti<sub>0.95</sub>O<sub>3</sub>-xSrTiO<sub>3</sub> multiphase ceramics followed the Lichtenegger mixture rules. The multiphase ceramic 0.98MgSn<sub>0.05</sub>Ti<sub>0.95</sub>O<sub>3</sub>-0.02SrTiO<sub>3</sub> sintered at 1330℃ for 4 h had excellent microwave dielectric properties (i.e.,  $\epsilon_r=19.32$ ,  $Q \times f=193.527$  THz,  $\tau_f=-2 \times 10^{-6}$ /℃).

**Key words:** microwave dielectric ceramic; multiphase ceramics; dielectric properties; quality factor

近年来, 微波介质陶瓷材料在手机通信、无线局域网络、卫星直播、全球定位系统等通讯领域得到了广泛应用<sup>[1]</sup>。为了提高通讯质量, 具有高品质因数的微波介质陶瓷材料日益受到人们重视<sup>[2]</sup>。MgTiO<sub>3</sub>陶瓷价格低廉、具有较高的品质因数( $\epsilon_r=16.8$ ,  $Q \times f=160$  THz,  $\tau_f=-50 \times 10^{-6}$ /℃)<sup>[3]</sup>, 引起了材料研究人员的关注, 因此, 对其进行了大量的研究。

Sohn等<sup>[4]</sup>和Huang等<sup>[5]</sup>研究发现采用Co<sup>2+</sup>和

Zn<sup>2+</sup>取代MgTiO<sub>3</sub>结构中A位的Mg<sup>2+</sup>, 通过晶格畸变和阳离子的尺寸效应可以有效地提高MgTiO<sub>3</sub>的品质因数<sup>[4]</sup>, 当掺杂量(摩尔分数)为5%时, 获得最佳的介电性能:Mg<sub>0.95</sub>Co<sub>0.05</sub>TiO<sub>3</sub>( $\epsilon_r=16.8$ ,  $Q \times f=230$  THz,  $\tau_f=-54 \times 10^{-6}$ /℃); Mg<sub>0.95</sub>Zn<sub>0.05</sub>TiO<sub>3</sub>( $\epsilon_r=17.1$ ,  $Q \times f=264$  THz,  $\tau_f=-40.3 \times 10^{-6}$ /℃)。Tseng等<sup>[6]</sup>采用Sn<sup>4+</sup>取代MgTiO<sub>3</sub>结构中B位的Ti<sup>4+</sup>, 可以提高陶瓷的相对密度, 从而提高MgTiO<sub>3</sub>的品质因数。当掺杂量为5%(摩尔分数)时, 最佳的介电性能为: $\epsilon_r=$

收稿日期: 2012-07-09。 修订日期: 2012-09-19。

基金项目: 江苏高校优势学科建设工程资助项目(PAPD); 江苏省高校自然科学基金(10KJB430008); 广东省科技计划项目; 广东省战略性新兴产业核心技术攻关(2011A091103002)。

第一作者: 龚志杰(1988—), 男, 硕士研究生。

通信作者: 张其土(1962—), 男, 博士, 教授。

Received date: 2012-07-09. Revised date: 2012-09-19.

First author: GONG Zhijie (1988-), male, Master candidate.

E-mail: gongzhijie1988@126.com

Correspondent author: ZHANG Qitu (1962-), male, Ph.D., Professor.

E-mail: njzqt@126.com

17.4,  $Q \times f = 322 \text{ THz}$ ,  $\tau_f = -54 \times 10^{-6}/$ 。虽然A位、B位的离子取代可以大幅提高 $\text{MgTiO}_3$ 的品质因数,但是对其谐振频率温度系数没有什么改善,仍为较大的负值。因此,采用具有正谐振频率温度系数的材料与 $\text{MgTiO}_3$ 复合,以调节其谐振频率温度系数。已经实际应用的是采用 $\text{CaTiO}_3$ 复合,当  $n(\text{Mg}) : n(\text{Ca}) = 95:5$ 时, $0.95\text{MgTiO}_3 - 0.05\text{CaTiO}_3$ 的介电性能为 $\varepsilon_r$ 约为21,  $Q \times f$ 约为56 THz,  $\tau_f$ 约为 $0 \times 10^{-6}/$ ,但是其烧结温度过高,需要1400~1450,并且 $Q \times f$ 值较低。

实验中采用Sn取代B位的Mg来提高 $\text{MgTiO}_3$ 的致密度及其品质因数。 $\text{SrTiO}_3$ <sup>[7]</sup> ( $\varepsilon_r = 190$ ,  $Q \times f = 4.2 \text{ THz}$ ,  $\tau_f = 1600 \times 10^{-6}/$ )与 $\text{CaTiO}_3$  ( $\varepsilon_r = 170$ ,  $Q \times f = 3.6 \text{ THz}$ ,  $\tau_f = 800 \times 10^{-6}/$ )相比,具有更高的 $Q \times f$ 值和更大的正谐振频率温度系数,因此,采用复合 $\text{SrTiO}_3$ 来调节其谐振频率温度系数,以期获得具有高品质因数和近零谐振频率温度系数的 $\text{MgTiO}_3$ 基微波介质陶瓷材料。

## 1 实验

### 1.1 样品制备

以高纯 $\text{Mg}(\text{OH})_2$ 、 $\text{TiO}_2$ 、 $\text{SnO}_2$ 和 $\text{SrCO}_3$ (均>99.9%,质量分数)为原料,采用传统固相法制备 $(1-x)\text{MgSn}_{0.05}\text{Ti}_{0.95}\text{O}_3 - x\text{SrTiO}_3$ 复相陶瓷。

按照 $\text{MgSn}_{0.05}\text{Ti}_{0.95}\text{O}_3$ 和 $\text{SrTiO}_3$ 的化学计量比分别称取原料,各自放入尼龙罐中,加入去离子水球磨12 h;取出烘干后,在1100预烧4 h;将预烧后的粉料按照 $(1-x)\text{MgSn}_{0.05}\text{Ti}_{0.95}\text{O}_3 - x\text{SrTiO}_3$  ( $x = 0.01 \sim 0.05$ ,摩尔分数)的配比称量,放入尼龙罐中,加水球磨12 h;烘干后,加入粉料总质量7%的PVA研磨造粒,然后压制成 $\phi 13 \text{ mm} \times 6 \text{ mm}$ 的圆柱状坯体,在1300~1390烧结4 h制得陶瓷样品。

### 1.2 表征

采用Archimedes法在室温下测试样品的体积密度。用D/Max 2500型X射线衍射仪分析样品的晶相组成。用JEM-5900型扫描电子显微镜观察样品表面形貌并用能谱仪对样品进行微区成分分析。采用Hakki-Coleman法<sup>[8]</sup>,使用Aglient公司8722ET型精密网络分析仪测量样品的介电性能。谐振频率温度系数通过下式进行计算:

$$\tau_f = \frac{f_{80} - f_{25}}{f_{25} \times (t_{80} - t_{25})} \quad (1)$$

式中: $f_{80}$ 为样品在80的谐振频率; $f_{25}$ 为样品在25的谐振频率。

## 2 结果与分析

### 2.1 物相分析

图1为 $(1-x)\text{MgSn}_{0.05}\text{Ti}_{0.95}\text{O}_3 - x\text{SrTiO}_3$  ( $x = 0.01 \sim 0.05$ )陶瓷在1330烧结的X射线衍射(XRD)谱。从图1中可见:样品的主晶相为 $\text{MgTiO}_3$ (JCPDS 06-0494),次晶相为 $\text{SrTiO}_3$ (JCPDS 35-0724),另外还有少量的 $\text{MgTi}_2\text{O}_5$ (JCPDS 35-0792)。随着x的增加, $\text{SrTiO}_3$ 的衍射峰在逐渐增强。 $\text{MgTiO}_3$ 为菱方晶系,钛铁矿结构,而 $\text{SrTiO}_3$ 为立方晶系,钙钛矿结构,并且 $\text{Mg}^{2+}$ 的离子半径为0.072 nm, $\text{Sr}^{2+}$ 的离子半径为0.144 nm<sup>[9]</sup>,两者相差较大,根据形成固溶体的离子半径比原则, $\text{MgTiO}_3$ 和 $\text{SrTiO}_3$ 两相不能形成固溶体。由于二者在高温下也不发生反应,故能够很好地复合。 $\text{MgTi}_2\text{O}_5$ 介电性能较差( $\varepsilon_r = 17.4$ ,  $Q \times f = 47 \text{ THz}$ ,  $\tau_f = -66 \times 10^{-6}/$ )<sup>[10]</sup>。 $\text{MgTi}_2\text{O}_5$ 制备过程中不希望获得的相,但是,通过固相法合成 $\text{MgTiO}_3$ 时,该相很难被完全消除<sup>[11]</sup>。

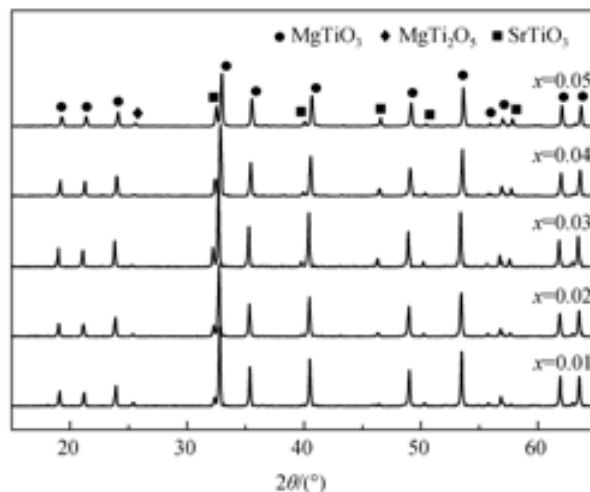


图1 在1330烧结 $(1-x)\text{MgSn}_{0.05}\text{Ti}_{0.95}\text{O}_3 - x\text{SrTiO}_3$ 陶瓷的XRD谱

Fig. 1 XRD patterns of  $(1-x)\text{MgSn}_{0.05}\text{Ti}_{0.95}\text{O}_3 - x\text{SrTiO}_3$  ceramics sintered at 1330

### 2.2 显微结构分析

图2为 $(1-x)\text{MgSn}_{0.05}\text{Ti}_{0.95}\text{O}_3 - x\text{SrTiO}_3$  ( $x = 0.01 \sim 0.05$ )陶瓷在1330烧结的SEM照片。从图2中可以看出:不同 $\text{SrTiO}_3$ 掺杂量的样品均已高度致密,几乎没有气孔,大晶粒呈多边形紧密排列,晶界清晰,大晶粒尺寸较均一,另有一些小晶粒较均匀地分布在样品中。随着 $\text{SrTiO}_3$ 掺杂量的增加,样品的大晶粒尺寸没有发生明显的变化,小晶粒的数量在逐渐增多,因此,这些小晶粒很有可能是 $\text{SrTiO}_3$ 。

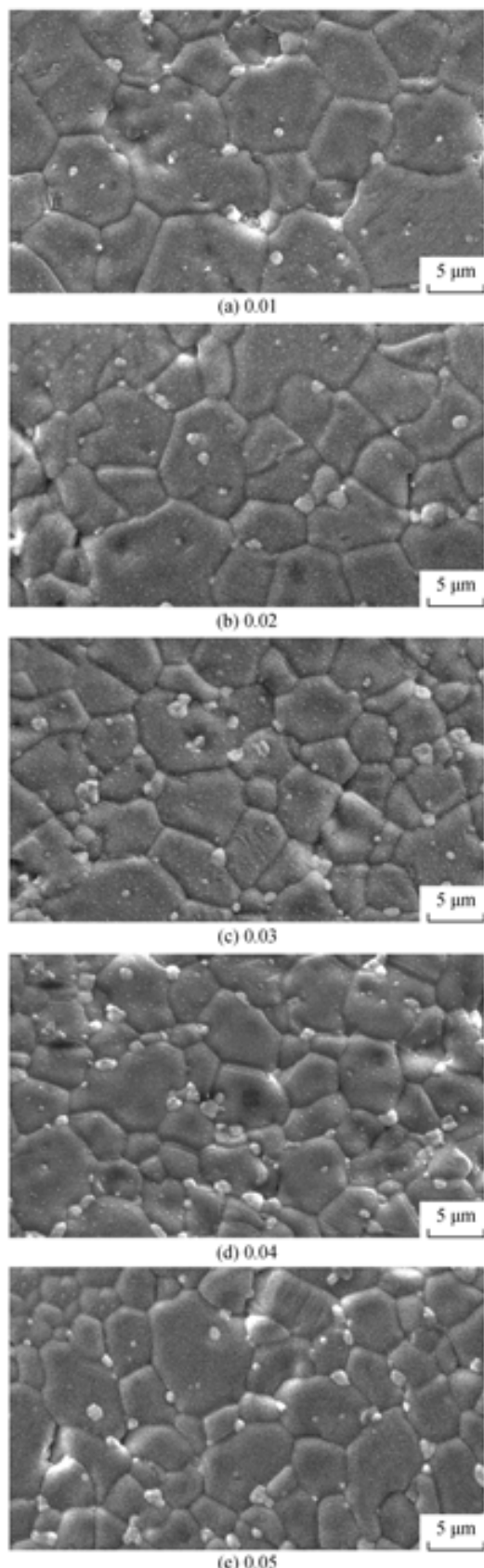
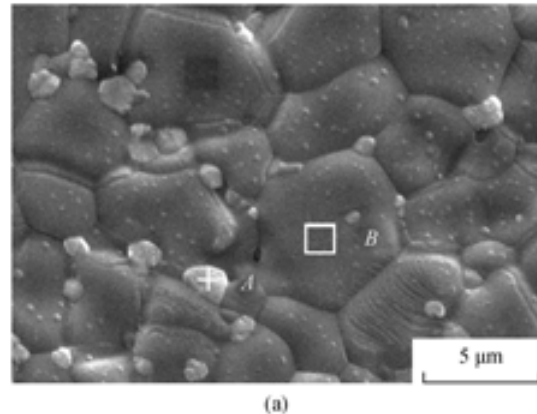


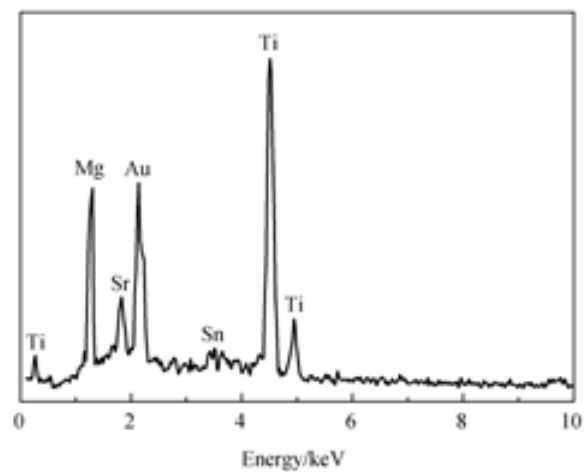
图2 1330烧结 $(1-x)$ MgSn<sub>0.05</sub>Ti<sub>0.95</sub>O<sub>3</sub>- $x$ SrTiO<sub>3</sub>陶瓷的SEM照片

Fig. 2 SEM micrographs of  $(1-x)$ MgSn<sub>0.05</sub>Ti<sub>0.95</sub>O<sub>3</sub>- $x$ SrTiO<sub>3</sub> ceramics sintered at 1300

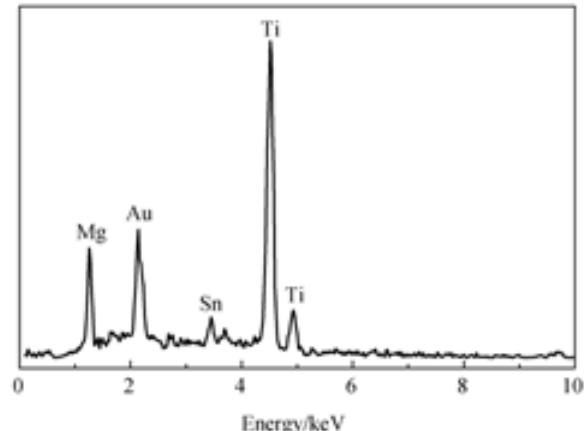
图3为掺杂4%SrTiO<sub>3</sub>的MgSn<sub>0.05</sub>Ti<sub>0.95</sub>O<sub>3</sub>陶瓷在1330烧结的EDS谱，可以看到：小晶粒中含有Mg、Ti、Sr、Sn4种元素，而大晶粒中则只含有Mg、Ti、Sn3种元素，未检测到Sr元素。结合图1中的XRD谱可知，小晶粒很有可能是由少量的固



(a)



(b) Spot A in Fig. 3(a)



(c) Area B in Fig. 3(a)

图3 在1330烧结MgSn<sub>0.05</sub>Ti<sub>0.95</sub>O<sub>3</sub>-0.04SrTiO<sub>3</sub>陶瓷的微区EDS谱

Fig. 3 EDS spectra of MgSn<sub>0.05</sub>Ti<sub>0.95</sub>O<sub>3</sub>-0.04SrTiO<sub>3</sub> ceramics sintered at 1330

溶了 Sn 离子的  $\text{MgTi}_2\text{O}_5$  和大量的  $\text{SrTiO}_3$  组成的小颗粒<sup>[12]</sup>，而大晶粒则为固溶了 Sn 离子的  $\text{MgTiO}_3$ 。为了进一步确定晶粒的组成，对点 A 和区域 B 进行了元素的定量分析，结果如表 1。从表 1 中可见：在点 A 中，主要组分为  $n(\text{Sr}):n(\text{Ti}) = 1:1$  的  $\text{SrTiO}_3$ ，同时含有少量固溶了 Sn 离子的  $n(\text{Mg}):n(\text{Ti}) = 1:2$  的  $\text{MgTi}_2\text{O}_5$ ；区域 B 为  $n(\text{Mg}):n(\text{Ti}) = 1:1$  的  $\text{MgSn}_{0.05}\text{Ti}_{0.95}\text{O}_3$ 。因此，小颗粒主要由  $\text{SrTiO}_3$  组成，同时也说明  $\text{SrTiO}_3$  和  $\text{MgTiO}_3$  不发生固溶，这与 XRD 谱得出的结论一致。

表 1  $\text{MgSn}_{0.05}\text{Ti}_{0.95}\text{O}_3-0.04\text{SrTiO}_3$  陶瓷中点 A 和区域 B(图 3a 中显示)的 EDS 结果

Table 1 EDS date of  $\text{MgSn}_{0.05}\text{Ti}_{0.95}\text{O}_3-0.04\text{SrTiO}_3$  for spot A and area B in Fig. 3a

Spot A		Area B	
Atom	Mole fraction/%	Atom	Mole fraction/%
Mg K	3.41	Mg K	28.95
Sn K	0.76	Sn K	1.42
Ti K	36.52	Ti K	27.56
Sr L	30.01	Sr L	0
O K	29.30	O K	42.08

### 2.3 微波介电性能分析

图 4a 为  $(1-x)\text{MgSn}_{0.05}\text{Ti}_{0.95}\text{O}_3-x\text{SrTiO}_3$  ( $x=0.01 \sim 0.05$ ) 复相陶瓷在 1 330 °C 烧结的体积密度和介电常数( $\epsilon_r$ )图。随着  $\text{SrTiO}_3$  含量的增加，样品的体积密度在逐渐增加。从 SEM 照片中可见，样品已高度致密，气孔对致密度的影响很小，因此，样品体积密度的增加，主要是由于  $\text{SrTiO}_3$  含量的增加，因为  $\text{SrTiO}_3$  的密度 (5.119 g/cm<sup>3</sup>) 大于  $\text{MgTiO}_3$  的密度 (3.894 g/cm<sup>3</sup>)。样品的介电常数随着  $\text{SrTiO}_3$  含量的增加呈线性增加，从 18.51 增加到 21.56。根据 Clausius-Mossotti 公式，单位体积内的离子极化率增加将提高样品的介电常数。由于  $\text{Sr}^{2+}$  具有较大的离子极化率，使得样品总的离子极化率在增加，从而使样品的介电常数一直增大。

图 4b 为  $(1-x)\text{MgSn}_{0.05}\text{Ti}_{0.95}\text{O}_3-x\text{SrTiO}_3$  ( $x=0.01 \sim 0.05$ ) 复相陶瓷在 1 330 °C 烧结的  $Q \times f$  值和谐振频率温度系数( $\tau_f$ )图。材料的微波介电损耗( $1/Q$ )包含材料本征损耗和非本征损耗，本征损耗取决于晶体本身<sup>[13]</sup>，而非本征损耗则与材料中的缺陷有关，如：气孔、第二相、晶粒的均一性、晶体缺陷等<sup>[14]</sup>。随着  $\text{SrTiO}_3$  含量的增加， $Q \times f$  值呈明显下降趋势(从 245.451 THz 降到 47.113 THz)，这是由于  $\text{SrTiO}_3$  的晶粒尺寸较小，复合后使得样品的晶粒尺

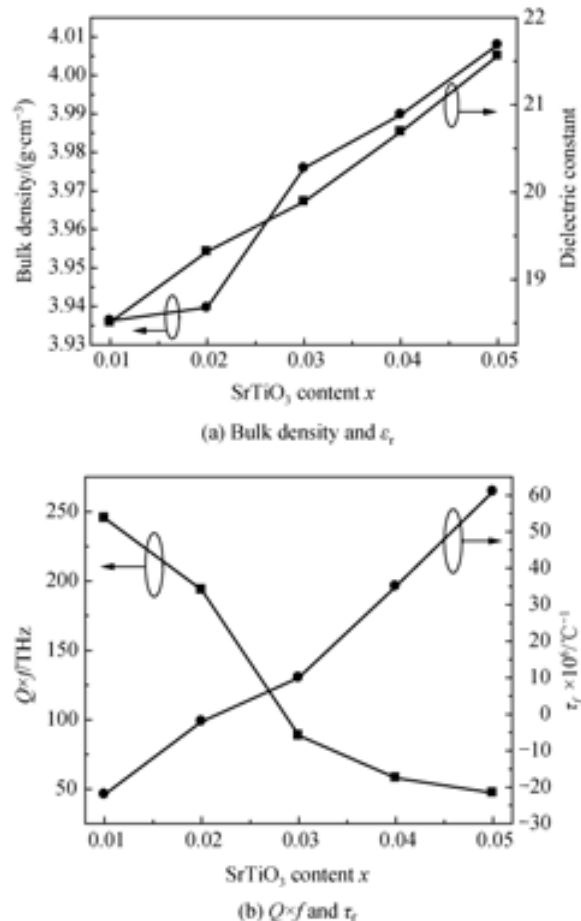


图 4  $(1-x)\text{MgSn}_{0.05}\text{Ti}_{0.95}\text{O}_3-x\text{SrTiO}_3$  陶瓷的体积密度与介电常数  $\epsilon_r$  和  $Q \times f$  与  $\tau_f$

Fig. 4 Bulk density and dielectric constant  $\epsilon_r$  and  $Q \times f$  and  $\tau_f$  of  $(1-x)\text{MgSn}_{0.05}\text{Ti}_{0.95}\text{O}_3-x\text{SrTiO}_3$  ceramics as a function of  $\text{SrTiO}_3$  content ( $x$ )

寸不均匀，两相晶界处产生大量缺陷，增加了样品中的非本征损耗，使得  $Q \times f$  值下降；谐振频率温度系数主要与材料的组成和第二相有关<sup>[15]</sup>。样品的  $\tau_f$  值随着  $\text{SrTiO}_3$  含量的增加呈线性增加， $\tau_f$  值由  $-22 \times 10^{-6}/^\circ\text{C}$  变为  $61 \times 10^{-6}/^\circ\text{C}$ 。这是由于  $\text{SrTiO}_3$  的  $\tau_f$  值为较大的正值  $1600 \times 10^{-6}/^\circ\text{C}$ ， $\text{MgSn}_{0.05}\text{Ti}_{0.95}\text{O}_3$  的  $\tau_f$  值为  $-54 \times 10^{-6}/^\circ\text{C}$ ，根据 Lichtenegger 混合定律<sup>[16]</sup>：

$$\tau_f = v_1 \tau_{f1} + v_2 \tau_{f2} \quad (2)$$

式中： $\tau_{f1}$ ， $\tau_{f2}$  为相应系统的介电常数； $v_1$ ， $v_2$  为原系统在复合系统中的体积分数， $v_1+v_2 = 1$ 。少量的  $\text{SrTiO}_3$  复合也会引起  $\tau_f$  值的较大变化，使得样品的  $\tau_f$  值变为正值。说明  $\text{SrTiO}_3$  复合可以有效调节  $\text{MgSn}_{0.05}\text{Ti}_{0.95}\text{O}_3$  的  $\tau_f$  值，在复合 2%  $\text{SrTiO}_3$  时，样品的  $\tau_f$  值为  $-2 \times 10^{-6}/^\circ\text{C}$ 。

根据以上研究， $0.98\text{MgSn}_{0.05}\text{Ti}_{0.95}\text{O}_3-0.02\text{SrTiO}_3$  复相陶瓷具有最佳的微波介电性能： $\epsilon_r = 19.32$ ， $Q \times f = 47.113$  THz， $\tau_f = -2 \times 10^{-6}/^\circ\text{C}$ 。

$f = 193.527 \text{ THz}$ ,  $\tau_f = -2 \times 10^{-6}/$ 。为了研究温度对0.98MgSn<sub>0.05</sub>Ti<sub>0.95</sub>O<sub>3</sub>-0.02SrTiO<sub>3</sub>陶瓷介电性能的影响,表2给出了0.98MgSn<sub>0.05</sub>Ti<sub>0.95</sub>O<sub>3</sub>-0.02SrTiO<sub>3</sub>陶瓷在不同温度下烧结的介电性能。随着温度的升高,样品的 $\tau_f$ 值变化不大,说明温度对样品 $\tau_f$ 值的影响很小。而样品的介电常数和 $Q \times f$ 值均呈现出先增大后减小的趋势,这与样品体积密度的变化趋势一致,且三者均在1330时达到极值。当烧结温度为1390时,导致部分晶粒生长过快,使得MgTiO<sub>3</sub>和SrTiO<sub>3</sub>2相不能很好地复合,形成大量气孔,从而使样品体积密度迅速下降,介电常数和 $Q \times f$ 值严重恶化。因此0.98MgSn<sub>0.05</sub>Ti<sub>0.95</sub>O<sub>3</sub>-0.02SrTiO<sub>3</sub>复相陶瓷的致密度是影响其介电常数和 $Q \times f$ 值的主要因素。

表2 在不同烧结温度0.98MgSn<sub>0.05</sub>Ti<sub>0.95</sub>O<sub>3</sub>-0.02SrTiO<sub>3</sub>陶瓷的介电性能

Table 2 Dielectric properties of 0.98MgSn<sub>0.05</sub>Ti<sub>0.95</sub>O<sub>3</sub>-0.02Sr-TiO<sub>3</sub> ceramics sintered at different temperatures

Sintering temperature/	Bulk density/ (g·cm <sup>-3</sup> )	Porosity/%	$\epsilon_r$	$Q \times f$ value/ THz	$\tau_f \times 10^6/$ -1
1300	3.89	5.4	18.96	141.103	-3
1330	3.94	3.9	19.32	193.527	-2
1360	3.92	4.2	19.06	111.816	-2
1390	3.83	11.2	18.18	39.166	-6

### 3 结 论

利用固相法制备了不同配比的(1-x)MgSn<sub>0.05</sub>Ti<sub>0.95</sub>O<sub>3</sub>-xSrTiO<sub>3</sub>复相陶瓷,通过调节x值,获得谐振温度频率系数 $\tau_f$ 近零的介质材料。SrTiO<sub>3</sub>和MgSn<sub>0.05</sub>Ti<sub>0.95</sub>O<sub>3</sub>在1330能很好地复合,当x=0.2时,获得最佳的介电性能: $\epsilon_r=19.32$ , $Q \times f=193.527 \text{ THz}$ , $\tau_f=-2 \times 10^{-6}/$ 。相对于0.95MgTiO<sub>3</sub>-0.05CaTiO<sub>3</sub>复相陶瓷,0.98MgSn<sub>0.05</sub>Ti<sub>0.95</sub>O<sub>3</sub>-0.02SrTiO<sub>3</sub>复相陶瓷烧结温度更低,具有较高的品质因数,将其作为一种微波介质陶瓷材料具有很好的应用前景。

### 参考文献:

- [1] 杨辉,张启龙,王家邦,等.微波介质陶瓷及器件研究进展[J].硅酸盐学报,2003,31(10): 965-973,980.

- YANG Hui, ZHANG Qilong, WANG Jiabang, et al. J Chin Ceram Soc, 2003, 31(10): 965-973, 980.  
[2] 彭森,吴孟强,肖勇,等.SrCO<sub>3</sub>掺杂对BMT陶瓷结构及介电性能的影响[J].硅酸盐学报,2012,39(12): 1947-1952.  
PENG Sen, WU Mengqiang, XIAO Yong, et al. J Chin Ceram Soc, 2012, 39(12): 1947-1952.  
[3] FERREIRA V M, AZOUGH F, BAPTISTA J L, et al. Dic 12: Magnesium titanate microwave dielectric ceramics [J]. Ferroelectrics, 1992, 133(1): 127-132.  
[4] SOHN J H, INAGUMA Y, YOON S O, et al. Microwave dielectric characteristics of ilmenite-type titanates with high  $Q$  values [J]. Jpn J Appl Phys, 1994, 33(9B): 5466-5470.  
[5] HUANG C L, LIU S S. Characterization of extremely low loss dielectrics (Mg<sub>0.95</sub>Zn<sub>0.05</sub>)TiO<sub>3</sub> at microwave frequency [J]. Jpn J Appl Phys, 2007, 46(1): 283.  
[6] TSENG Ching-Fang, HSU Cheng-Hsing. A new compound with ultra low dielectric loss at microwave frequencies [J]. J Am Ceram Soc, 2009, 92(5): 1149-1152.  
[7] BALL C J, BEGG B D, COOKSON D J, et al. Structures in the system CaTiO<sub>3</sub>/SrTiO<sub>3</sub> [J]. J Solid State Chem, 1998, 139(2): 238-247.  
[8] HAKKI B W, COLEMAN P D. A dielectric resonator method of measuring inductive capacities in the millimeter range [J]. Microwave Theory and Techniques, IRE Transactions on, 1960, 8(4): 402-410.  
[9] SHANNON R D. Revised effective ionic radii and systematic studies of interatomic distances in halides and chalcogenides [J]. Acta Crystallographica Section A: Crystal Physics, Diffraction, Theoretical and General Crystallography, 1976, 32(5): 751-767.  
[10] SHIN H K, SHIN H, CHO SY, et al. Phase evolution and dielectric properties of MgTiO<sub>3</sub>-CaTiO<sub>3</sub> based ceramic sintered with lithium borosilicate glass for application to low temperature co-fired ceramics [J]. J Am Ceram Soc, 2005, 88(9): 2461-2465.  
[11] HUANG C L, PAN C L. Low-temperature sintering and microwave dielectric properties of (1-x)MgTiO<sub>3</sub>-xCaTiO<sub>3</sub> ceramics using bismuth addition [J]. Jpn J Appl Phys, 2002, 41(2A): 707-711.  
[12] CHO W W, KAKIMOTO K, OHSATO H. High-Q microwave dielectric SrTiO<sub>3</sub> doped MgTiO<sub>3</sub> materials with near-zero temperature coefficient of resonant frequency [J]. Jpn J Appl Phys, 2004, 43(9): 6221-6224.  
[13] 石峰.Ba(Zn<sub>1/3</sub>Nb<sub>2/3</sub>)O<sub>3</sub>微波介质陶瓷介电性能的研究[D].杭州:浙江大学,2003.  
SHI Feng. The study of dielectric properties of Ba(Zn<sub>1/3</sub>Nb<sub>2/3</sub>)O<sub>3</sub> microwave dielectric ceramics [Dissertation, in Chinese]. Hangzhou: Zhejiang University, 2003.  
[14] FREEER R, AZOUGH F. Microstructural engineering of microwave dielectric ceramics [J]. J Euro Ceram Soc, 2008, 28(7): 1433-1441.  
[15] HUANG C L, WANG J J, CHANG Y P. Dielectric properties of low loss (1-x)(Mg<sub>0.95</sub>Zn<sub>0.05</sub>)TiO<sub>3</sub>-xSrTiO<sub>3</sub> ceramic system at microwave frequency [J]. J Am Ceram Soc, 2007, 90(3): 858-862.  
[16] LICHTENECKER K. Dielectric constant of natural and synthetic mixtures [J]. Physics (Z), 1926, 27: 115.

## 原位反应法制备 Cr<sub>2</sub>AlC-Fe 复合材料

陈新华，翟洪祥，王文娟，黄振莺  
(北京交通大学，北京 100044)

**摘要：**采用原位反应法制备了 Cr<sub>2</sub>AlC-Fe 系复合材料，并采用热分析、X 射线衍射、扫描电子显微镜和三点弯曲实验，研究了原位反应的烧结工艺对产物和显微结构的影响，以及对原料中 Cr<sub>2</sub>AlC 的含量对复合材料性能的影响。结果表明：通过高温原位反应，原料中 Cr<sub>2</sub>AlC 发生了分解，形成了网络状陶瓷增强结构，所制备的复合材料具有较好的强度和韧性，且随着 Cr<sub>2</sub>AlC 含量的增加，复合材料的强度也在增加，但断裂韧性逐渐下降。当 Cr<sub>2</sub>AlC 的体积分数达到 30% 时，复合材料的抗弯强度达 1417 MPa。

**关键词：**复合材料；原位反应；烧结；弯曲行为

中图分类号：TB333 文献标志码：A 文章编号：0454-5648(2013)01-

网络出版时间： 网络出版地址：

### Fabrication of Cr<sub>2</sub>AlC Fe-based Composites by *in-situ* Reaction Method

CHEN Xinhua, ZHAI Hongxiang, WANG Wenjuan, HUANG Zhenying

(Center of Materials Science and Engineering, School of Mechanical and Electronic Control Engineering,  
Beijing Jiaotong University, Beijing 100044)

**Abstract:** A Cr<sub>2</sub>AlC-Fe composite, which could have potential applications in nuclear energy industry as engineering materials, was synthesized by an *in-situ* reaction method. The *in-situ* reactions between Cr<sub>2</sub>AlC and Fe at different temperatures and ratios were analyzed by thermogravimetric analysis-differential thermal analysis, X-ray diffraction and scanning electron microscopy, respectively. The effect of Cr<sub>2</sub>AlC content on the bending behaviors was investigated. The results show that Cr<sub>2</sub>AlC can *in-situ* react with Fe, and decompose to form chromium carbide. The synthesized composite exhibits a higher flexural strength and a greater fracture toughness at room temperature.

**Key words:** based composites; in situ reaction; sintering; bending behaviors

### 1 Introduction

Combine with the unique desirable properties of a single metal or ceramic material and offsetting each other's deficiencies, composites can be used as the engineering materials for extreme environment of nuclear energy industry, mining industry, chemical and metallurgical industry and so on.<sup>[1-3]</sup> The reinforcing ceramic particulates include Al<sub>2</sub>O<sub>3</sub>, TiC, Si<sub>3</sub>N<sub>4</sub>, WC, etc.<sup>[4-8]</sup> Although those traditional ceramic reinforcements own high strength, they have low fracture toughness, poor wetting, inconsistency of linear expansion coefficient with iron, and are hard to be machined by using normal tools.

Recently, Cr<sub>2</sub>AlC and related composites have attracted increasing attention,<sup>[9-13]</sup> which belong to a new

type of ternary structures advance ceramics so called MAX phase. Compared with traditional ceramic reinforcing agents, these kinds of ceramics possess unique crystal laminated structure as graphite. In the Cr<sub>2</sub>AlC crystal structure, the Cr atoms and C atoms form two common edges Cr<sub>6</sub>C tetrahedron with strong ionic bond are separated by Al atomic planes,<sup>[14]</sup> and the link between Al atomic planes and Cr<sub>6</sub>C tetrahedron are weak Cr-Al metallic bond.<sup>[15-16]</sup> This structure lead the Cr<sub>2</sub>AlC phase combinational properties of both metals and ceramics, such as low density, high modulus, easy machinability, good electrical and thermal conductivity, excellent thermal shock and high-temperature oxidation resistance, but also can react with Fe by the technique of in situ reaction method,<sup>[17-19]</sup> which is a process where

收稿日期：2012-04-23。 修订日期：2012-09-25。

基金项目：国家“863”项目(2006AA03Z527)。

第一作者：陈新华(1983—)，男，博士研究生。

Received date: 2012-04-23. Revised date: 2012-09-25.

First author: CHEN Xinhua (1983-), male, Ph.D., Candidate.

E-mail: 07116311@bjtu.edu.cn

reinforcements are synthesized in metallic matrix by chemical reactions, and ensured the introduction of chemical bonding force in the interface of the reinforcements and the metal matrix, and the high performance bonding will make the external applied stress transferred from the matrix to the reinforcements. Zhang *et al.*<sup>[20]</sup> nosed out that the reaction between Cu and Ti<sub>3</sub>AlC<sub>2</sub> form TiC<sub>x</sub> and Cu(Al) above 950 °C. Our previous work<sup>[21–24]</sup> shows that the incorporation of Ti<sub>3</sub>SiC<sub>2</sub> or Ti<sub>3</sub>AlC<sub>2</sub> with Cu increase the strength and modulus as well as wear resistance without the loss of conductivity and meet the requirements of applications in electrical sliding contacts in high-speed railway. In fact, similar reactions also exist between the Cr<sub>2</sub>AlC with Fe matrix.

Hence, this paper intends to report on processing and property of Fe-based Metal Matrix Composites (MMCs) using the Cr<sub>2</sub>AlC, which is a type member of the MAX phase ceramics, as precursor in the raw material. By using this *in-situ* reaction method, the Cr<sub>2</sub>AlC ceramic particles might decompose to fine chromium carbide reinforcing agents. Different from the traditional direct synthesis methods, this method has several advantages, such as the better link between the reinforcing agents with the matrix, and the easier distributed evenly of the reinforcing agents, and so on.

## 2 Experimental

Reduced iron powders (purity 99.5%, size < 74 μm, Beijing Chemical Reagent Company) and Cr<sub>2</sub>AlC powders (purity > 97%, average size 5.197 μm, the details can be found elsewhere<sup>[10]</sup>) are mixed for 10 h in plastic cans to ensure homogeneous reactant mixtures. The Cr<sub>2</sub>AlC particle powders size measurement was performed on laser diffraction particle size analyzer (Mastersizer 2000, Malvern, Britain). Then, the mixed powders were hot-pressed (HP) at 1 300 °C under 30 MPa for 30 min in flowing argon gas. The flexural strength of the composites was tested by three-point bending method by GB/T 6569–1986, and the fracture toughness was tested by single edge notched and three-point bending method (SENB). The final samples were cut into blocks with dimensions of 3 mm × 4 mm × 36 mm for bending tests, of 4 mm × 6 mm × 36 mm for SENB tests, the both tests were performed on a universal testing machine (ZWICK, Z005) at a loading speed of 0.5 mm/min. According to the standard force and displacement from the universal testing machine, the bending strength and fracture toughness of the composites are calculated from following equations respectively:

$$R_{tr} = \frac{3FL}{2bh^2} \quad (1)$$

$$K_{IC} = \frac{3FL}{2bh^2} \times \sqrt{a} \left( 1.93 - 3.07 \frac{a}{h} + 14.53 \frac{a^2}{h^2} - 25.07 \frac{a^3}{h^3} + 25.80 \frac{a^4}{h^4} \right) \quad (2)$$

where  $R_{tr}$  and  $K_{IC}$  are the flexural strength and fracture toughness of the composites respectively,  $F$  is the force required to the fracture,  $L$  is the distance between the fulcrums,  $b$  and  $h$  are the width and thickness of the samples respectively,  $a$  is the crack length of the composites, here is 2.8 mm.

After the bending tests, the specimens were analyzed by a scanning electron microscopy (SEM)(JSM-6460).

## 3 Results and discussion

Figure 1 shows the TG–DTA curve of 30%Cr<sub>2</sub>AlC/70%Fe system and the DTA curves of pure Fe. In the TG–DTA curve of 30%Cr<sub>2</sub>AlC/70%Fe system, there are no obvious changes in the weight during the reaction between Cr<sub>2</sub>AlC and Fe, which indicates that there is no obvious change in the weight during the reaction between Cr<sub>2</sub>AlC and Fe. In the DTA curve 30%Cr<sub>2</sub>AlC/70%Fe system, two endothermic peaks sat 763.5 °C and 914.5 °C can be observed. For the endothermic peaks, compare to the DTA curves of pure Fe, one can notice that almost same endothermic peaks at 770.21 and 915.24 °C are observed in the DTA curves of Fe. Hence, it can be concluded that two endothermic peaks at 763.1 °C and 913 °C are probably ascribed to the phase transition of Fe.

Indeed, according to the Fe–Al phase diagrams,<sup>[25]</sup> it can be seen the magnetic transition temperature ( $T_c$ ) of Fe at 770 °C and the transformation of α-Fe to γ-Fe at 912 °C are in good agreement with our results here. Above 914.5 °C, the endothermic reaction is predominant and there was no new obvious peak. The different phase compositions at different temperatures were made certain by the analyzing of XRD.

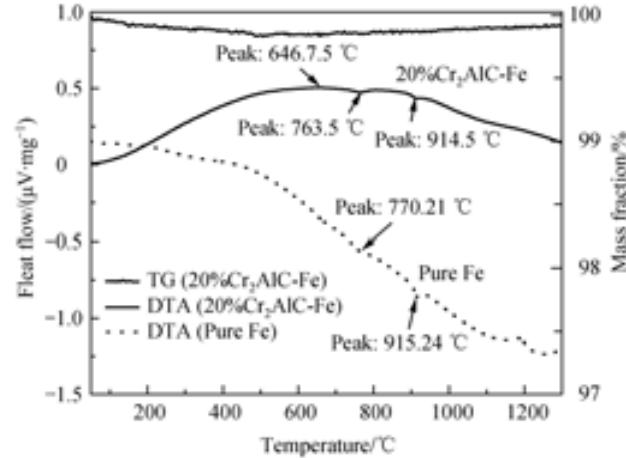


Fig. 1 TG–DTA curves for 30% Cr<sub>2</sub>AlC/70%Fe and DTA curves for pure Fe powder in argon atmosphere

Figure 2 shows the XRD patterns of samples of 30%Cr<sub>2</sub>AlC/70%Fe composites sintering at the temperatures from 1 000 °C to 1 400 °C under 30 MPa for 30 min. The results show that, when the sintering temperature is between 1 000 to 1 300 °C, the peaks from Cr<sub>2</sub>AlC dis-

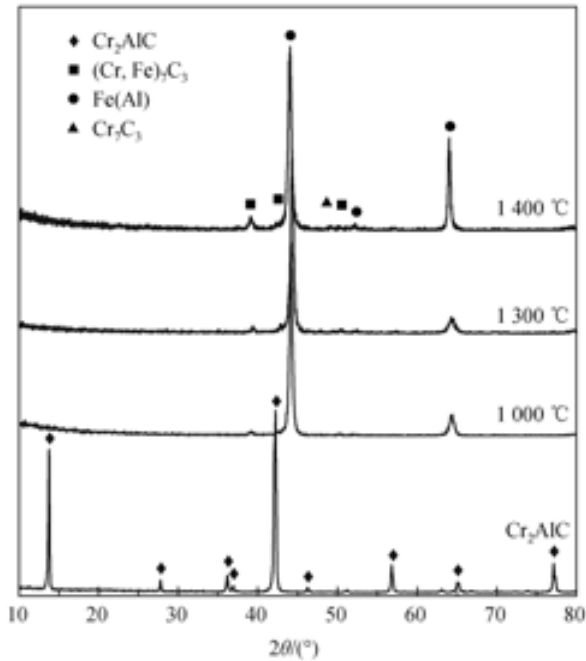


Fig. 2 XRD patterns of Cr<sub>2</sub>AlC powders and samples of 30%Cr<sub>2</sub>AlC/70%Fe composites sintered at 1 000 to 1 400

peared and the main phases were stability of (Cr,Fe)<sub>7</sub>C<sub>3</sub> and Fe (Al). As the sintering temperature continued rise to 1 400 , the intensity of the diffraction peaks from Fe (Al) was growing substantially, and great contraction deformation has emerged in the samples after sintering at 1 400 , this phenomenon indicating that the ceramic segregation had occurred at this high temperature. So the temperature from 1 000 to 1 300 is the appropriate sintering temperature range.

Figure 3 shows the XRD patterns of samples of Cr<sub>2</sub>AlC-Fe mixtures with different Cr<sub>2</sub>AlC contents after sintered at 1 300 under 30 MPa for 30 min. When the Cr<sub>2</sub>AlC contents in the mixtures below 30%, no new phases can be detected besides Fe (Al) and (Cr, Fe)<sub>7</sub>C<sub>3</sub>. As the Cr<sub>2</sub>AlC contents increasing to 50%, the diffraction peaks from Cr<sub>7</sub>C<sub>3</sub> became higher. The main reason of the reactions can be contributed to the *in-situ* reaction between Cr<sub>2</sub>AlC and Fe. This *in-situ* reaction can be described as this: At high sintering temperature, Al atoms can strip from Cr<sub>2</sub>AlC due to the weak Cr-Al metallic bond in Cr<sub>2</sub>AlC, and dissolve in the metal matrix, forming Cr<sub>7</sub>C<sub>3</sub> grains and Fe (Al) solid solution. At the same time, Fe will through into the ceramics particles by the Al vacancies. When the Cr<sub>2</sub>AlC contents increasing to 50%, the liquid Fe are insufficient and results in some Cr<sub>7</sub>C<sub>3</sub> phase remaining. The reaction can be described as following:

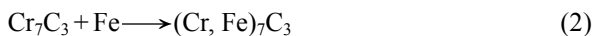
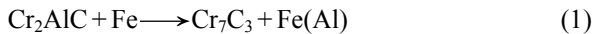


Figure 4 shows the microstructure of samples of 30%

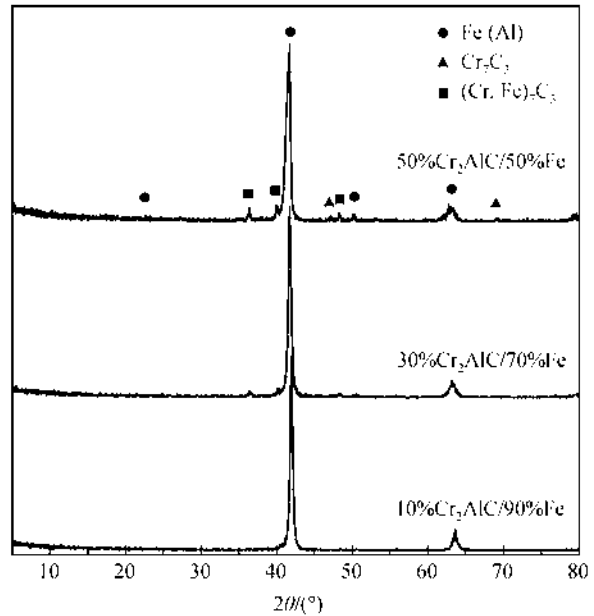
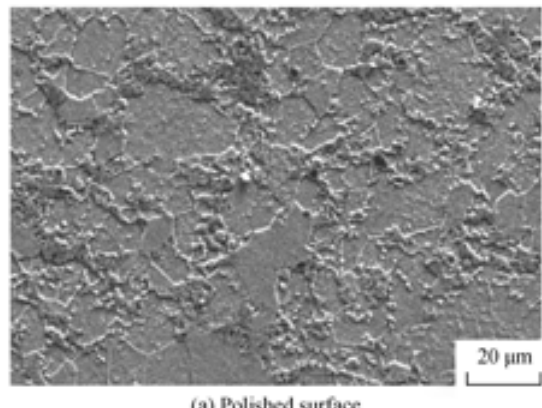
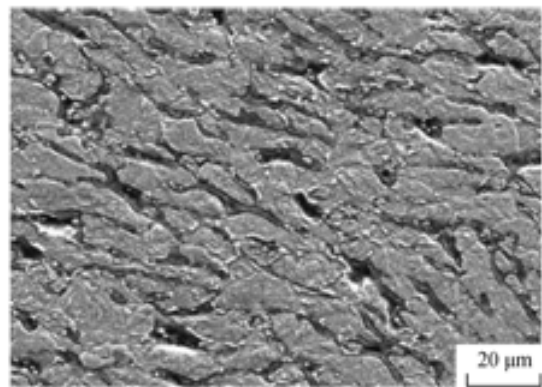


Fig. 3 XRD patterns of samples of Cr<sub>2</sub>AlC-Fe mixtures with different Cr<sub>2</sub>AlC contents after sintered at 1 300 for 30 min



(a) Polished surface



(b) Polished surface which was etched in nital

Fig. 4 Microstructure of samples of 30%Cr<sub>2</sub>AlC/70%Fe sintered at 1 300 under 30 MPa for 30 min

Cr<sub>2</sub>AlC/70%Fe sintered at 1 300 under 30 MPa for 30 min. Choose a notable ceramics area in a bulk 30%Cr<sub>2</sub>AlC/70%Fe composites' polished surface, and its SEM

image shows as Fig. 4(a). In the composites, the ceramic particulates are uniformly distributed in the matrix, and the ceramic particulates with shapes of needle, spindle, and flake. Figure 4(b) is a representative SEM image of the bulk 30%Cr<sub>2</sub>AlC/70%Fe system composites' polished surface which was etched in nital. This typical micrograph exhibits that the composites with a compact texture, and the ceramic particulates are uniformly distributed in the Fe matrix with the average thickness size of 1.3 μm, form a hard continuous skeleton. This structure can be contribute to the microstructure genetic effects from the superimposed shape of the platelet microcrystalline Cr<sub>2</sub>AlC in the of Cr<sub>2</sub>AlC polycrystalline grains.

The sample of 30%Cr<sub>2</sub>AlC/70%Fe sintered at 1300 for 30 min in argon atmosphere, and its flat well-polished surface analyzed by EDS are shown in Fig. 5. It clearly shows that the Cr<sub>2</sub>AlC particles almost turned into Cr<sub>7</sub>C<sub>3</sub>. We can also observe that Fe had diffused into the Cr<sub>2</sub>AlC particles, Al, Cr and C can be detected in the Fe matrix.

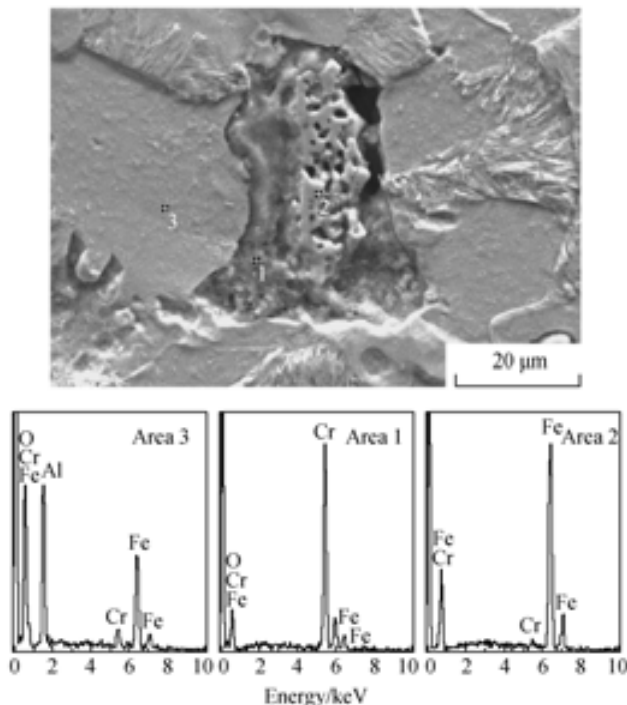


Fig. 5 EDX of samples of 30%Cr<sub>2</sub>AlC/70%Fe sintered at 1300 under 30 MPa for 30 min

Figure 6 shows the relationship between the flexural strength, fracture toughness and the volume content of Cr<sub>2</sub>AlC for Cr<sub>2</sub>AlC-Fe composites sintered at 1300 for 30 min. The flexural strength of the sample was increased greatly, but the fracture toughness was decreased while raising Cr<sub>2</sub>AlC content. When the Cr<sub>2</sub>AlC content was 50% in the starting materials, the flexural strengths of 50%Cr<sub>2</sub>AlC/50%Fe can reach 1417.05 MPa, however, its fracture toughness drop to 18 MPa·m<sup>1/2</sup>. A most remarkable feature is the strengths of Cr<sub>2</sub>AlC-Fe composites not only much stronger than the strengths of pure Fe bulk, but

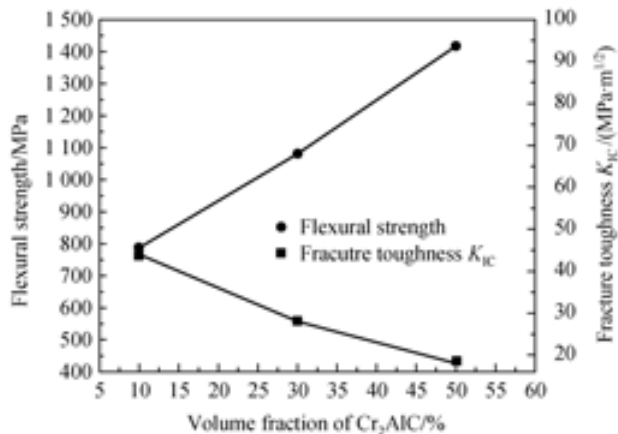


Fig. 6 Relationship between the flexural strength, fracture toughness and the volume content of Cr<sub>2</sub>AlC for Cr<sub>2</sub>AlC-Fe composites sintered at 1300 for 30 min

also much stronger than the strengths of Cr<sub>2</sub>AlC bulk (which flexural strengths is about 378 MPa). This phenomenon can be contributed to the hard continuous skeleton microstructure and strong interface bonding between the reinforce particulates and the metal matrix in the composites.

Figure 7 shows the typical bending site specimen photograph of 30%Cr<sub>2</sub>AlC/70%Fe sample sintered at 1300 for 30 min after the bending tests. A lot of slip bands are formed in the matrix at about 45° with respect to draw axis. This result indicates that the interfacial bond between the ceramic reinforcements and metal matrix are strong. After in situ reaction, the chemical bond is formed in the interface between the chromium carbide particulates and matrix. During deformation, the ceramic particles not only can resist the passing dislocations, but also can induce drag force to the grain boundaries of the matrix. As a result, the external applied stress will be transferred from the matrix to chromium carbide particulates, and undoubtedly, the load bearing capacity of the composites with

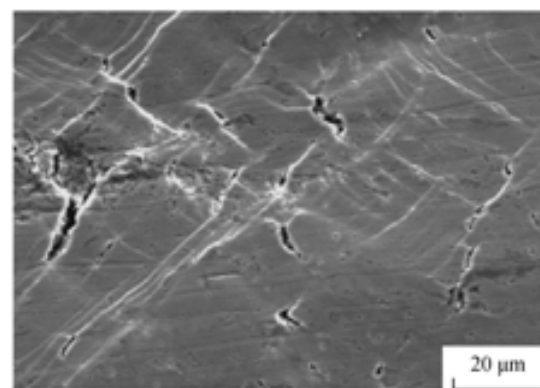


Fig. 7 Typical bending site specimen photograph of 30%Cr<sub>2</sub>AlC/70%Fe sample sintered at 1300 for 30 min after bending tests

more ceramic reinforcement will be greater during the period of elastic deformation.

## 4 Conclusions

The chromium carbide reinforces Fe (Al) composites can be prepared by *in-situ* reaction method using Cr<sub>2</sub>AlC powders as precursor. The *in-situ* reaction between Cr<sub>2</sub>AlC and Fe completed above 1 000 °C, and the products main phases keep stable in the 1 000–1 300 °C sintering temperature range. As the Cr<sub>2</sub>AlC content increasing, the flexural strength of the sample is increased greatly, but the toughness is decreased.

### References:

- [1] ABENOJAR J, VELASCO F, TORRALBA J M, et al. Reinforcing 316 L stainless steel with intermetallic and carbide particles [J]. Mater Sci Eng A-struct, 2002, 335(1-2): 1–5.
- [2] CLYNE T W, WITHERS P J. An introduction to metal matrix composites [M]. Cambridge: Cambridge University Press, 1993.
- [3] DAS K, BANDYOPADHYAY T K, DAS S. A review on the various synthesis routes of TiC reinforced ferrous based composites [R]. J Mater Sci, 2002, 37(18): 3881–3892.
- [4] KONOPKA K, OZIBLO A. Microstructure and the fracture toughness of the Al<sub>2</sub>O<sub>3</sub>–Fe composites [J]. Mater Charact, 2001, 46(2-3): 125–129.
- [5] ZEBARJAD S M, SAJJADI S A. Dependency of physical and mechanical properties of mechanical alloyed Al–Al<sub>2</sub>O<sub>3</sub> composite on milling time [J]. Mater Design, 2007, 28(7): 2113–2120.
- [6] NI Z F, SUN Y S, XUE F, et al. Microstructure and properties of austenitic stainless steel reinforced with in situ TiC particulate [J]. Mater Design, 2011, 32(3): 1462–1467.
- [7] IBRAHIM I A, MOHAMED F A, LAVERNIA E J. Particulate reinforced metal matrix composites – a review [J]. J Mater Sci, 1991, 26(5): 1137–1156.
- [8] ARIK H. Effect of mechanical alloying process on mechanical properties of  $\alpha$ -Si<sub>3</sub>N<sub>4</sub> reinforced aluminum-based composite materials [J]. Mater Design, 2008, 29(9): 1856–1861.
- [9] BARSOUM M W. The M<sub>N+1</sub>AX<sub>N</sub> Phases: A new class of solids: Thermodynamically stable nanolaminates [J]. Prog Solid State Chem, 2000, 28: 201–81.
- [10] LI S B, YU W B, ZHAI H X, et al. Mechanical properties of low temperature synthesized dense and fine-grained Cr<sub>2</sub>AlC ceramics. J Eur Ceram Soc, 2011, 31(1-2): 217–24.
- [11] GUPTA S, FILIMONOV D, ZAITSEV V, et al. Study of tribofilms formed during dry sliding of Ta<sub>2</sub>AlC/Ag or Cr<sub>2</sub>AlC/Ag composites against Ni-based superalloys and Al<sub>2</sub>O<sub>3</sub> [J]. Wear, 2009, 267(9–10): 1490–1500.
- [12] WANG J Y, ZHOU Y C. Dependence of elastic stiffness on electronic band structure of nanolaminate M<sub>2</sub>AlC (M = Ti, V, Nb, and Cr) ceramics [J]. Phys Rev B, 2004, 69(21): 214111.
- [13] YING G B, HE X D, LI M W, et al. Effect of Cr<sub>7</sub>C<sub>3</sub> on the mechanical, thermal, and electrical properties of Cr<sub>2</sub>AlC [J]. J Alloy Compd, 2011, 509(31): 8022–8027.
- [14] CUI S X, WEI D Q, HU H Q, et al. First-principles study of the structural and elastic properties of Cr<sub>2</sub>AlX (X = N, C) compounds [J]. J Solid State Chem, 2012, 191: 147–152.
- [15] LIN Z J, ZHOU Y C, LI M S. Synthesis, microstructure, and property of Cr<sub>2</sub>AlC [J]. J Mater Sci Technol, 2007, 23(6): 721–746.
- [16] YANG Z J, LINGHU R F, CHENG X L, et al. First-principles investigations on the electronic, elastic and thermodynamic properties of Cr<sub>2</sub>MC (M = Al, Ga) [J]. Acta Phys Sin-Ch Ed, 2012, 61(4).
- [17] SHEHATA F, FATHY A, ABDELHAMEED M, et al. Preparation and properties of Al<sub>2</sub>O<sub>3</sub> nanoparticle reinforced copper matrix composites by in situ processing [J]. Mater Design, 2009, 30(7): 2756–2762.
- [18] TJONG S C, MA Z Y. Microstructural and mechanical characteristics of in situ metal matrix composites [J]. Mater Sci Eng R, 2000, 29(3–4): 49–113.
- [19] CHEN X H, ZHAI H X, SONG P F, et al. Reaction behavior of Ti<sub>3</sub>AlC<sub>2</sub> with Fe at high temperature [J]. Rare Metal Mater Eng, 2011(S1): 499–502.
- [20] ZHANG J, WANG J Y, ZHOU Y C. Structure stability of Ti<sub>3</sub>AlC<sub>2</sub> in Cu and microstructure evolution of Cu–Ti<sub>3</sub>AlC<sub>2</sub> composites [J]. Acta Mater, 2007, 55(13): 4381–4390.
- [21] AI M X, ZHAI H X, TANG Z Y. Interformational exfoliation of Ti<sub>3</sub>AlC<sub>2</sub> induced by Cu [J]. Key Eng Mater, 2007, 336–338: 1371–1373.
- [22] ZHANG Y, SUN Z, ZHOU Y. Cu/Ti<sub>3</sub>SiC<sub>2</sub> composite: a new electrofriction material [J]. Mater Res Innov, 1999, 3(2): 80–84.
- [23] ZHAI H X, AI M X, HUANG Z Y, et al. Unusual microstructures and strength characteristics of Cu/Ti<sub>3</sub>AlC<sub>2</sub> cermets [J]. Key Eng Mater, 2007, 336–338: 1394–1396.
- [24] ZHANG Z L, ZHAI H X, ZHOU Y, et al. Preparation of composites from Al and Ti<sub>3</sub>AlC<sub>2</sub> and its tribo-chemistry reactions against low carbon steel [J]. Key Eng Mater, 2008, 368–372: 989–991.
- [25] BAKER H, OKAMOTO H. ASM Handbook [M]. USA: ASM International Handbook Committee, 1992.